Tearing Mode Instability due to Anomalous Resistivity

FURUYA, Atsushi
Interdisciplinary Graduate School of Engineering Sciences, Kyushu University

ITOH, Sanae-I.
Research Institute for Applied Mechanics, Kyushu University

YAGI, Masatoshi
Research Institute for Applied Mechanics, Kyushu University

https://doi.org/10.15017/6767930

出版情報：九州大学応用力学研究所所報. 119, pp.61-74, 2000-09. Research Institute for Applied Mechanics, Kyushu University
バージョン：
権利関係：

Tearing Mode Instability due to Anomalous Resistivity

Atsushi FURUYA*1, Sanae -I. ITOH*2and Masatoshi YAGI*2
E-mail of corresponding author: *atsushi@post.riam.kyushu-u.ac.jp*

(Received April 1, 2000)

Abstract

Tearing mode instability in the presence of microscopic turbulence is investigates. The effects of microscopic turbulence on tearing mode are taken as drags which are calculated by one-point renormalization method and mean-field approximation. These effects are reduced to effective diffusivities in reduced MHD equations. Using these equations, the stability analyses of the tearing mode are performed. It is shown that a finite amplitude of fluctuation enhances the growth rate of tearing mode. For very high values of turbulent diffusivities, marginally stable state exists. The effects of each turbulent diffusivity on mode stability are examined near marginal stability boundary. Parameter dependence of the resistive ballooning mode turbulence on tearing mode is analyzed as an example.

Key words : *tearing mode instability, microscopic turbulence, anomalous resistivity, turbulent diffusitity, resistive ballooning mode turbulence*

1. Introduction

Various types of collapse phenomena are observed [1] in high temperature plasmas, which sometimes bring a serious limitation on the tokamak performance. For the achievement of high performance in fusion plasmas, it is necessary to understand the physical mechanism of collapse phenomena. At the same time, collapse phenomena are challenging issues of the physics for understanding the dynamics of nonequilibrium system. The characteristic features of the collapse phenomena in high temperature plasmas include:

(i)the sudden growth of symmetry-breaking electromagnetic perturbations;

(ii)bursts of energy, momentum and particles across magnetic surface;

(iii)avalanches, i.e. the propagation of the collapses;

(iv)the possible periodic occurrences of bursts, and also their unpredictability.

Especially for the investigation of the physical mechanism, many experiments related to the sudden growth of perturbations have been performed.

In JET, experiments have been carried out focussed on the sawtooth problem [5]. It is observed that the m=1/n=1 perturbation precedes the decay of the central electron temperature. In the initial stage of a fast temperature crash, this mode grows very slowly. At some instant, the helical deformation abruptly starts to grow where the growth rate discontinuously jumps to the level of $\gamma \sim 10^5 s^{-1}$. The similar phenomenon is observed in Heliotron-E device [6]. Plasmas in the torsatron/Heliotron configuration are confined by the magnetic field produced by external coils. Therefore, the instability is related to the plasma pressure (gradients), not to the internal current if the plasma pressure is not extremely high. In the case of the internal disruption, m=2/n=1 mode grows abruptly before the crash. The maximum value of the growth rate ranges about $10^4 s^{-1}$. In these experiments, a large amount of the pressure and pressure gradient changes does not occur, nevertheless the mode rapidly grows associated with discontinuous and large change of the growth rate. The sudden growth of the collapses has been widely observed which are listed in Table 1.

In the conventional theoretical models based on the linear instability, the temporal change of the linear growth rate γ_L should follow the change of the global plasma parameters. Namely, the abrupt change of the growth rate requires the corresponding changes of the global parameters such as safety factor q, pressure gradient p' and so on. Therefore, a certain mechanism which is beyond the linear theory's is needed to explain such a mechanism for the acceleration of the trigger mode.

Theoretical approaches for such problems have been proposed based on nonlinear instability. Diamond et al. considers that the overlap of magnetic islands generates the magnetic stochasticity and its magnetic fluctua-

*1 Interdisciplinary Graduate School of Engineering Sciences, Kyushu University
*2 Research Institute for Applied Mechanics, Kyushu University

Name	Observed response	Time scale	Trigger mode	Precursor mode	Note
Sawtooth	$T_e n_e$ $\Delta q \sim 0.05$	<100 μs	$m/n = 1/1$ etc (?)	$m/n = 1/1$	No full-reconnection $q(0) < 1$
Partial sawtooth	As above	←	←	←	←
Disruption (thermal quench)	T_e	10–100 μs	$m/n = 1/1$ 'erosion'	$m/n = 2/1$ 3/1 etc	Density limit, $q = 2, 3$
High-β collapse (tokamak)	T_e (T_i)	<100 μs	$n \gg 1$ ballooning	$m/n = 1/1$ etc	$\beta \sim \beta_c^{MHD}$
Internal collapse (Heliotron)	T_e	<100 μs	$m/n = 2/1$ interchange	$m/n = 2/1$	
ELMs (type-I)	$T_e T_i n_e$	10–100 μs	$n \gg 1$	—	$\alpha \sim \alpha_c^{MHD}$
X-event	$\chi_i T_i$	<100 μs	—	—	High-T_i mode
BLM	∇T_e	<100 μs	$m/n = 3/1$ Infernal?	—	High-β_p mode
MTE	∇V_φ	<100 μs	$n \gg 1$	—	Prohibits VH-mode
CHS burst	$\phi(r)$	few 100 μs	$m/n = 2/2$	$m/n = 2/1$	NBI injection
IRE	ℓ_i				Low-aspect radio tokamak

Table 1 Crash events, precursors and triggering modes. Abbreviations: ELMs(edge-localized modes), MTE(momentum transfer events), BLM(barrier-localized mode), IRE(internal reconnection events). (cited from Ref. [1])

tions play a role of anomalous resistivity [8]. The nonlinear processes are analyzed by one-point renormalization method [9] and the effect of background fluctuations is reduced to the form of anomalous resistivity. This has been applied to the case of major disruption. However the abrupt growth of trigger mode which has the single helicity has not been explained.

A hierarchical model has been introduced to analyze collapse phenomena where physical phenomena are considered to be separated into three scales, i.e., transport's one, MHD mode's one and microscopic turbulence's one [10]. Figure 1 shows the schematic illustration of the hierarchical model. These three groups interact with each other through the nonlinearity even though the linear interaction is little. In this study, a part of the hierarchical model that is the interaction between the MHD and turbulence, is derived as a prototype. From MHD class, tearing mode with a single helicity is chosen and for the microscopic turbulence, a resistive ballooning mode turbulence is considered. The back reaction from MHD mode to turbulent mode is not taken into account. The effect from the microscopic turbulence to the MHD mode is introduced as the transport coefficients where the nonlinear interactions are treated by one-point renormalization method. The model equations for MHD mode with the influence from microscopic turbulence are derived. Using this model equation, the dynamics of tearing mode is examined.

The organization of this paper is as follows: In Chapter 2, characteristic feature of collapse phenom-

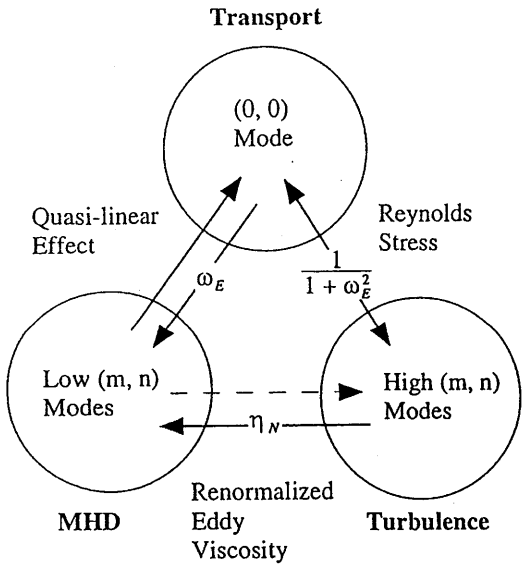

Fig. 1 The schematic illustrate of a hierarchical model. Physical phenomena are considered to be separated into three scales; namely transport, MHD mode and microscopic turbulence scales. They interact with each other. m is a poloidal mode number and n is a toroidal mode number.

ena and the problems of conventional theoretical model based on linear instability analysis are reviewed. Theoretical approaches which explain nonlinear acceleration mechanisms are also reviewed. In Chapter 3, the model equations which represent the global MHD mode with the effect of the microscopic turbulence are derived. Using these model equations, the tearing mode is numerically analyzed in Chapter 4. Summary and discussions are given in Chapter 5.

2. Reviews

2.1 Collapse Phenomena

Several examples of fast time-scale phenomenon of its occurrence and the nonlinear nature are reviewed in this section. These characteristics of collapse phenomena are widely observed and these are widely reviewed in Ref [1]. Especially, the sudden growth of trigger mode is seen at various collapse phenomena as shown in Table 1.

The sawtooth is one of well-known collapse phenomena and is characterized by a relatively slow buildup of the temperature on the axis which happens in millisecond time-scale, and followed by a fast temperature crash. Also, many experiments at JET have been carried out focussed on the sawtooth problem [5]. Figure 2 shows the electron temperature at the center and the topology of a fast temperature crash, which are derived from soft X-ray (SXR) emission measurement. The crash occurs as a rapidly growing helical perturbation of the plasma core, also with $m = 1/n = 1$, followed by a flattening of temperature and density profiles across the central plasma, the entire event having a time-scale of $\sim 100\mu s$. This perturbation which leads to the collapse event is called a precursor [7].

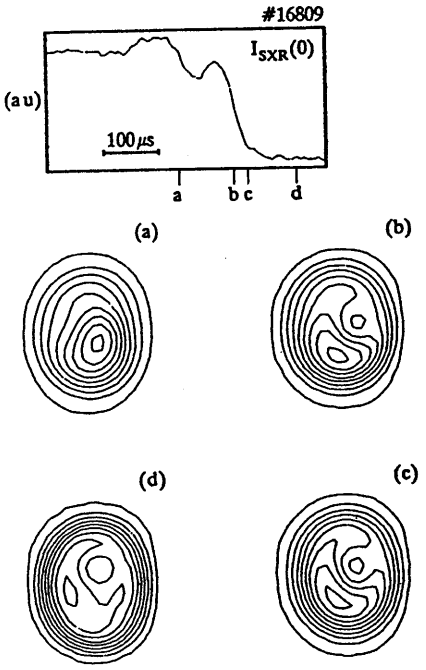

Fig. 2 The Soft X-ray measurement of the electron temperature at the center and two-dimensional reconstruction of the rapid sawtooth collapse in JET. It occurs in $100/mus$. (cited from Ref. [5])

Figure 3 shows the growth of the trigger mode, as deduced from the displacement of the peak of tomographically inverted SXR profiles (for three sawtooth collapses in different discharges) . The initial noise level is $\sim 1cm$ and the displacement rises out of this noise with a growth rate $\sim (25\mu s)^{-1}$. Extrapolation of this growth backwards in time yields a displacement equal to the Debye length, perhaps the smallest realistic scale for the instability, on a time-scale of order $\sim 100\mu s$. In contrast, conventional models based on the linear theory involve in quantities such as safety factor q or beta value β which would require time-scales $\sim 100ms$ to generate such large growth rates. In experiments, such a large

change of global parameters is not observed.

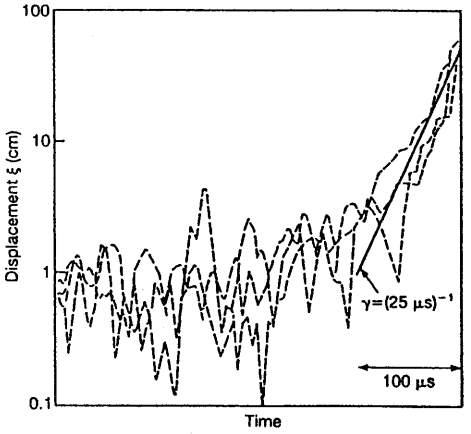

Fig. 3 Displacement of the soft X-ray emission peak, derived from two-dimensional tomographic reconstructions, during fast sawtooth collapse. Experimental results for three cases are illustrated. The data show that a growth rate of $(25\mu s)^{-1}$ is achieved even before the displacement is large enough to be detected above the experimental noise. (cited from Ref. [5])

Crash phenomena have been observed on the Heliotron-E device [6].

Figure 4 illustrates an internal disruption which occurs near the $q = 2$ surface. An $m = 2$ mode grows abruptly, triggering the internal disruption within about $100 \sim 300\mu s$. The experimental conditions are $B_0 = 1.9T$, $\bar{n_e} = 1 \sim 10 \times 10^{19} m^{-3}$, $T_e(0) = 300 \sim 2000eV$, and $T_i(0) = 200 \sim 1000eV$. A two-dimensional reconstruction for the soft X ray emissivity ϵ_{SX} is obtained by a Fourier-Bessel expansion technique with a maximum poloidal mode number of 3 and a radial mode number of 8. Figure 5(a) shows that the $m = 2$ component $\epsilon_{SX,m=2}$ grows near the $q = 2$ surface. The time evolution of the perturbation amplitude,

$$\tilde{A}_{m=2} \propto \epsilon_{SX,m=2} \qquad (1)$$

is followed in time. The growth rate γ_{obs} is determined as a function of time. It is shown that the $m = 2$ mode grows abruptly just before the crash within a few $100\mu s$ to a few ms. The maximum value of the growth rate ranges $10^4 s^{-1}$. Because plasmas in the Heliotron-E device are currentless and confined by the external coil, it has been recognized that the plasma pressure (gradient)

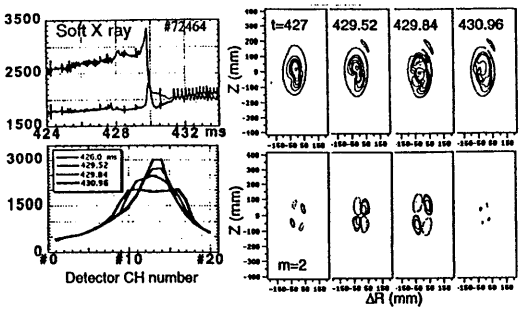

Fig. 4 Typical example of an internal disruption. integrated soft X ray profiles and tomographically reconstructed emissivity contours are shown during the crash phase. The m=2 component is also shown. Before the crash it localized close to the magnetic axis, and the the location departs from the axis, which indicates that the $q = 2$ surface changes at the crash. (cited from Ref. [6])

is the primary origin of the dynamical behavior. In order to find an onset condition for the mode to grow, the relation between γ and $\nabla\epsilon_{SX}|_{q=2}$ has been investigated and the result is shown in Figure 5(b). The result shows that there is no critical value for $\nabla\epsilon_{SX}|_{q=2}$ for the mode to grow and that the hysteresis relation exists between the growth rate and the global parameters.

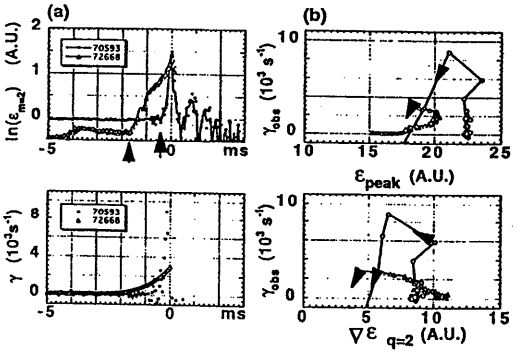

Fig. 5 Time evolution of $ln(\epsilon_{m=2})$ and γ_{obs} for two typical crash cases (a). The change of the growth rate is illustrated in (b). The abrupt increment of the growth rate is observed. (cited from Ref. [6])

2.2 Theoretical approach

In the conventional theoretical models based on linear instability analysis, the temporal change of the linear growth rate γ_L is dictated by the transport time scale. If one represents the growth rate by the global plasma parameters, the time change is expressed as

$$\frac{\partial \gamma_L}{\partial t} = \frac{\partial \gamma_L}{\partial q}\frac{\partial q}{\partial t} + \frac{\partial \gamma_L}{\partial \beta}\frac{\partial \beta}{\partial t} + \cdots \qquad (2)$$

The deviates $\partial\gamma_L/\partial q$, $\partial\gamma_L/\partial\beta$, etc are finite and γ_L is a smooth function global parameters. If the resistivity is the main cause of the dissipation, the typical time scale with which the growth of the island proceeds, is estimated as

$$\gamma \sim \frac{1}{(\tau_{Ap}\tau_R)^{1/2}}, \qquad (3)$$

where τ_R is the resistive diffusion time and τ_{Ap} is the poloidal Alfven transit time.

In the previous section, we review the characteristic feature of the sudden growth of symmetry-breaking perturbations. These observations most clearly illustrate the incompleteness of the picture based on the linear instability analysis. This means that a certain mechanism which is beyond the linear theory's is needed to explain such a mechanism for the acceleration of the trigger mode. Recently the theoretical approach to such problems has been proposed based on nonlinear instability analysis [8, 11]. In this section, the theoretical approach which explains the nonlinear acceleration mechanism is reviewed.

The nonlinear acceleration of the MHD mode caused by the stochastization of field lines is explained in Ref [11]. In this analysis, the following nonlinear processes are considered. The magnetic stochasticity resulting from the interaction of the fundamental m=1/n=1 mode with the mode of other periodicities enhances the effective electron and ion viscosities. The enhanced electron viscosity leads to an increase of the growth rate. The temporal evolution of the magnetic perturbation is shown in Figure 6. When the stochasticity condition is satisfied, the mode has the large growth rate. This means that microscopic fluctuations affect the global MHD mode and accelerate the instability.

An analytic theory of turbulence in reduced resistive magnetohydrodynamics is developed and applied to the major disruption in Ref [8]. Figure 7 shows the numerical results calculated for the major disruption. Figure 7(a) shows the temporal evolution of each magnetic island width. At the same time, the growth rate of m=3/n=2 mode is shown in Figure 7(b).

The initial equilibrium is chosen to be linearly unstable to the m=2/n=1 and m=3/n=2 resistive tearing modes. These modes grow exponentially in time until the width of their magnetic islands becomes comparable to that of the resistive tearing layer. The evolution of the instability enters the so-called Rutherford phase [12] where magnetic islands grow algebraically. As the m=2/n=1 and m=3/n=2 islands grow larger, the nonlinear interaction through the m=5/n=3 mode, which tends to accelerate the growth of the m=3/n=2 mode, occurs. Finally, the m=2/n=1 and m=3/n=2 islands overlap, triggering the occurrence of disruptive phenomenon due to the stochasticity. The sequence of phenomena leading to the final disruptive phase is depicted.

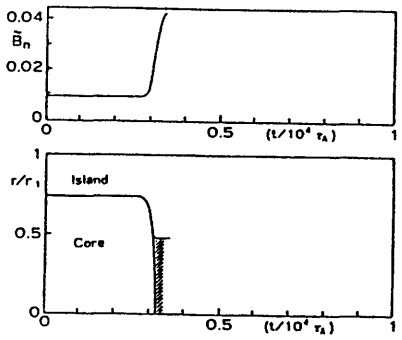

Fig. 6 The temporal evolution of the magnetic perturbation in the case of the sawtooth crash. When the stochasticity condition is satisfied, the mode has large growth rate. (cited from Ref. [11])

These nonlinear interactions are treated by one-point renormalization method. The direct interactions of the test mode with background fluctuations are reduced to anomalous diffusivities, and the anomalous tearing mode growth rate is given as

$$\gamma \sim \left(\sum_{k'} k_\theta'^2 |\phi_{k'}|^2\right)^{\frac{3}{8}} (\Delta')^{\frac{1}{2}}. \qquad (4)$$

which means that the background fluctuations contribute to the anomalous resistivity and accelerate through the nonlinearity. This analytical model is in good agreement with the computational results in the final phase of the major disruption shown in Figure 8. This is one of theoretical models which explains the mode acceleration mechanism, however, the rapid growth of trigger mode with a single helicity has not explicitly shown.

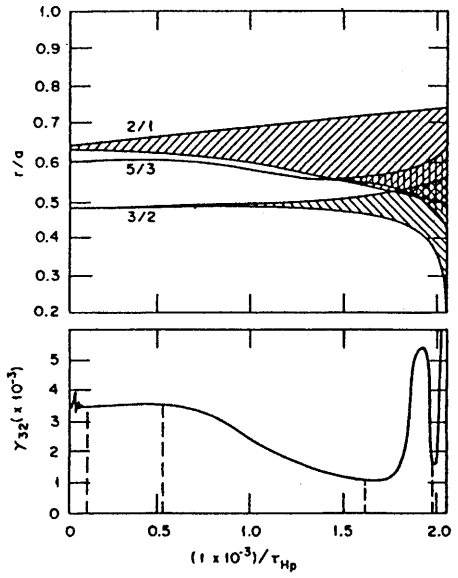

Fig. 7 The calculations are performed in such way that the various physical effects appears as a sequence of events. (a) The radial extent of three of magnetic islands. (b) The instantaneous growth rate of the $m = 3/n = 2$ mode. The overlap of magnetic islans of m=2/n=1 and m=5/n=3 generates the magnetic stochasticity and accelerates the groeth of m=3/n=2 mode. (cited from Ref. [8])

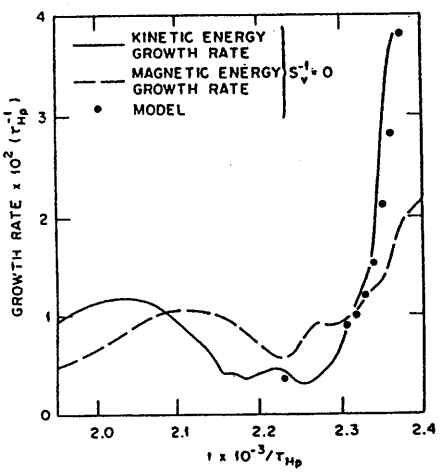

Fig. 8 The growth rate of the $m = 3/n = 2$ mode as obtained from the model is compared with the numerical calculation. (cited from Ref. [8])

2.2.1 Hierarchical model for plasma transport

In high temperature plasmas, there co-exists multi-scale dynamics, for example, macroscopic dynamics ($\sim a$) and microscopic dynamics ($\sim \rho_i$, $\sim \delta_e$), where a is a minor radius, ρ_i is an ion gyro radius and δ_e is an electron skin depth. Empirically, there are observed not only 'gyro-Bohm' like transport which is interpreted that the transport occurs as the local ($k \sim \rho_i^{-1}$) and diffusive phenomena, but also 'Bohm' like transport which could be caused by the transient, non-local $k \sim a$, and/or non-diffusive phenomena. The self-organized structure in high temperature plasma has the multi-dimensional nature. Typical examples of one dimensional structure are the electric field bifurcation and the interface dynamics, etc and of three dimensional structure are the island and the vortex and so on. The statistisity of plasma turbulence shows both the deterministic and probabilistic (chaos, intermittency) nature. To treat such problems, there are presently two approaches. As an approach from the microscopic view, a direct numerical simulation (DNS) is used which strongly depends on 'power computing'. Another one from the macroscopic point of view is the large eddy simulation (LES) with a hierarchical transport model. In this section, we discuss the concept of hierarchical model for plasma turbulence [10].

A large eddy simulation (LES) model which is discussed here consists of a hierarchy, i.e., three classes of time and spatial scales, that is transport, MHD, and turbulence. These classes are considered to be categorized by the poloidal and toroidal mode number, (m,n). A (0,0) mode represents the global transport, low (m,n) modes represent MHD behavior and high (m,n) modes represent turbulent fluctuations. Mutual interactions between three classes are possible via nonlinearities such as a Reynolds stress [13], a renormalized eddy viscosity and so on. Figure 1 shows the schematic view of hierarchical model.

A typical example of two hierarchical model is the one for transport and turbulence such as a transport model with a turbulent eddy viscosity and a predator-pray model [13] . In the latter model, Reynolds stress plays an important role, i.e., the shear flow suppression of turbulence via Reynolds stress leads to the improvement of transport.

3. Model equations

In this chapter, we present theoretical model equations for the global MHD mode in the presence of microscopic turbulence i.e. a model with two hierarchies,

where the effect of microscopic turbulence on the global MHD mode is considered.

3.1 Reduced MHD equations

A toroidal plasma of major and minor radii R_0 and a with an ambient magnetic field $\boldsymbol{B_0}$ is considered in the cylindrical coordinates (r, θ, z). Figure 9 shows the schematic view of coordinate system.

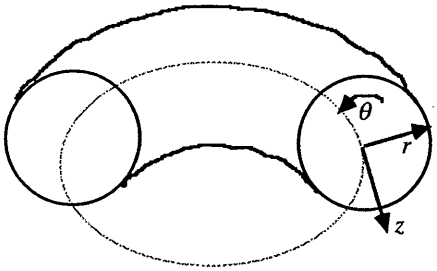

Fig. 9 Schematic view of coordinate system. The direction of each coordinate in toroidal plasma is shown.

To investigate the interaction between the global MHD mode and the microscopic turbulent mode, we start from the high-beta reduced MHD equations [14] which consist of the equation of motion :

$$\frac{\partial}{\partial t}\nabla_\perp^2\phi+\nabla_\parallel\nabla_\perp^2 A-\mu_c\nabla_\perp^4\phi-(\boldsymbol{b_0}\times\boldsymbol{\kappa})\cdot\nabla p+[J_0,A] = -[\phi,\nabla_\perp^2\phi]+[A,\nabla_\perp^2 A], \quad (5)$$

Ohm's law :

$$\frac{\partial}{\partial t}A+\nabla_\parallel\phi-\eta_c\nabla_\perp^2 A=[A,\phi], \quad (6)$$

and the energy balance equation :

$$\frac{\partial}{\partial t}p-\chi_c\nabla_\perp^2 p+[\phi,p_0]=-[\phi,p]. \quad (7)$$

The variables $\{\phi, A, p\}$ are perturbations of electrostatic potential, vector potential parallel to $\boldsymbol{b_0}$ and pressure. $\boldsymbol{b_0}$ is the unit vector which is parallel to the main magnetic field $\boldsymbol{B_0}$. $\{\mu_c, \eta_c, \chi_c\}$ are collisional viscosity, resistivity and thermal conductivity. The bracket $[,]$ represents the Poisson's bracket which is defined as $[F,G]\equiv(\nabla_\perp F\times\nabla_\perp G)\cdot\boldsymbol{b_0}$. $\boldsymbol{\kappa}$ is the magnetic curvature. The equilibrium pressure and current density are represented by p_0 and J_0, respectively. These variables are normalized as follows;

$$\frac{\epsilon v_A}{a}t\to t,\quad \frac{r}{a}\to r,\quad \frac{z}{R_0}\to z,$$
$$\frac{\phi}{B_0\epsilon a v_A}\to\phi,\quad \frac{A}{\epsilon a B_0}\to A,\quad \frac{\mu_0}{B_0^2\epsilon}p\to p, \quad (8)$$
$$\frac{\eta_c}{\mu_0\epsilon a v_A}\to\eta_c,,\frac{\mu_c}{n_0 m_i\epsilon a v_A}\to\mu_c,\frac{\chi_c}{\epsilon a v_A}\to\chi_c,$$

where v_A is Alfven velocity, n_0 is particle density and $\epsilon = a/R_0$ is the inverse aspect ratio. The right hand sides of these equations (5)-(7), which are represented by the Poisson's bracket, are the quadratic nonlinear terms for the perturbations $\{\phi, A, p\}$. Through these terms, the microscopic turbulence have an influence on the global MHD mode.

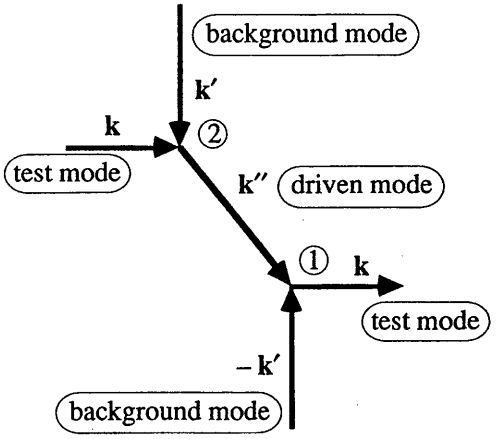

Fig. 10 Schematic explanation of nonlinear interaction. Interaction of a test mode $\boldsymbol{k}$ with a background turbulence $\boldsymbol{k'}$ induces a driven mode $\boldsymbol{k''}$. The back interaction drives the test mode $\boldsymbol{k}$.

4. Renormalization of nonlinearity

A part of nonlinear interactions are renormalized as eddy viscosities based on one-point renormalization method [8, 9, 15]. In this method, the following nonlinear processes are considered which is shown in Figure 10. We take a test mode(denoted by $\boldsymbol{k}$) which represents a global MHD mode, and calculate an interaction with a microscopic background turbulence mode which is denoted by $\boldsymbol{k'}$. This interaction generates a driven mode which is denoted by $\boldsymbol{k''}$ $(\boldsymbol{k''}=\boldsymbol{k'}+\boldsymbol{k})$. These wavenumbers have a relation $|\boldsymbol{k''}|, |\boldsymbol{k'}| \gg |\boldsymbol{k}|$. Then, the driven mode interacts with the background mode, and this back reaction contributes to the test mode. Considering this process of nonlinear interaction, the direct interaction of test mode with background turbulence is taken into account and is renormalized. We assume that the background turbulence is given, so that we do not solve the equations for the background mode $\boldsymbol{k'}$.

For the simplicity, the basic equations (5)-(7) are

symbolically rewritten as

$$(\partial_T + \mathcal{L})\,\mathcal{F} = N, \tag{9}$$

where ∂_T is an operator which includes the time derivative. $\mathcal{L}$ is a linear operator which represents the spatial structure. $\mathcal{F}$ denotes the perturbation. The explicit forms are given as follows,

$$\mathcal{F} = \begin{pmatrix} \phi \\ A \\ p \end{pmatrix},\ \partial_T = \frac{\partial}{\partial t}\begin{pmatrix} \nabla_\perp^2 & 0 & 0 \\ 0 & 1 & 0 \\ 0 & 0 & 1 \end{pmatrix},$$

$$\mathcal{L} = \begin{pmatrix} -\mu_c\nabla_\perp^4 & \nabla_\parallel\nabla_\perp^2 + J_0'\nabla_\theta & -(\boldsymbol{b_0}\times\boldsymbol{\kappa})\cdot\nabla \\ \nabla_\parallel & -\eta_c\nabla_\perp^2 & 0 \\ p_0'\nabla_\theta & 0 & -\chi_c\nabla_\perp^2 \end{pmatrix},$$

$$N = \begin{pmatrix} N_1 \\ N_2 \\ N_3 \end{pmatrix} = \begin{pmatrix} [A, \nabla_\perp^2 A] - [\phi, \nabla_\perp^2\phi] \\ [A,\phi] \\ [\phi, p] \end{pmatrix}.$$

In the first step, the equation (9) is solved for the test mode. The nonlinear term for the test mode N_k is calculated as

$$\begin{aligned} N_{1k} &= \sum_{k'} [A_{k'}, \nabla_\perp^2 A_{k''}] + [A_{k''}, \nabla_\perp^2 A_{k'}] \\ &\quad + [\phi_{k'}, \nabla_\perp^2\phi_{k''}] + [\phi_{k''}, \nabla_\perp^2\phi_{k'}] \\ N_{2k} &= \sum_{k'} [A_{k'}, \phi_{k''}] - [A_{k''}, \phi_{k'}] \\ N_{3k} &= \sum_{k'} -[\phi_{k'}, p_{k''}] + [\phi_{k''}, p_{k'}] \end{aligned}$$

This nonlinear term N_k is a summation over the products of driven modes and background turbulence modes. We assume the following parity for variables $\{\phi, A, p\}$ from basic equations (5)-(7)

$$\phi_{-k} = -\phi_k, A_{-k} = A_k, p_{-k} = p_k. \tag{10}$$

In the next step, equation (9) is solved for the driven mode $\boldsymbol{k''}$. The nonlinear term $N_{k''}$ for the driven mode $\boldsymbol{k''}$ is divided into two part; one is a contribution from the nonlinear coupling between a test mode $\boldsymbol{k}$ and a background mode $\boldsymbol{k'}$ and the other nonlinear interaction is approximated by $\Gamma_{k''}\mathcal{F}_{k''}$, where $\Gamma_{k''}$ is a nonlinear operator which excludes the self-action of background mode. Namely, equation of the driven mode is reduced to

$$(\partial_T + \mathcal{L} + \Gamma_{k''})\,\mathcal{F}_{k''} = \begin{pmatrix} (k'^2 - k^2)\left([A_{k'}, \nabla_\perp^2 A_k] - [\phi_{k'}, \nabla_\perp^2\phi_k]\right) \\ [\phi_{k'}, A_k] + [\phi_k, A_{k'}] \\ -[\phi_{k'}, p_k] - [\phi_k, p_{k'}] \end{pmatrix} \tag{11}$$

Using a local approximation, the equation for the driven mode is solved for $\mathcal{F}_{k''}$ of equation (11) and substituted to the nonlinear term of the test mode N_k. By this procedure, the nonlinear contribution to the test mode is expressed in terms of the background fluctuations. For the simplicity, only the diagonal elements of the nonlinear terms of the test mode are kept. Using a mean-field approximation, which assumes that the same averaged coefficients are used for the nonlinear terms of the background mode, and the diffusion approximation [15, 16], the following model equations for the global MHD mode are derived:

$$\frac{\partial}{\partial t}\nabla_\perp^2\phi + \nabla_\parallel\nabla_\perp^2 A - \mu_c\nabla_\perp^4\phi + ik_\theta g p + [J_0, A] = \mu_N\nabla_\perp^4\phi, \tag{12}$$

$$\frac{\partial}{\partial t}A + \nabla_\parallel\phi - \eta_c\nabla_\perp^2 A = \eta_N\nabla_\perp^2 A, \tag{13}$$

$$\frac{\partial}{\partial t}p - \chi_c\nabla_\perp^2 p + [\phi, p_0] = \chi_N\nabla_\perp^2 p, \tag{14}$$

where g represents the effective curvature due to the magnetic field and is defined as $g \equiv 2cos\theta$ in cylindrical coordinates (r, θ, z). Here g is approximated as a constant to analyze the tearing mode, which excludes the ballooning nature of the mode. The nonlinear terms of basic equations (5)-(7) are reduced to the effective turbulent diffusivities, $\{\mu_N, \eta_N, \chi_N\}$. They are the renormalized viscosity, resistivity and thermal conductivity, and are represented by the wave number and the amplitude of microscopic background turbulence. Explicit forms of these coefficients are given as follows;

$$\begin{aligned} \mu_N &= \sum_{k'} \frac{1}{3\gamma_\mu'}\frac{|k_\perp'\phi_{k'}|^2}{2K} \\ &\quad + \frac{1}{\gamma_\eta'}\left(1 - \frac{k_\parallel'k_\perp' + k_\parallel'k_\theta'\frac{dJ_0}{dr}}{k_\perp'\gamma_\mu'\gamma_\eta'}\right)\frac{|k_\perp'A_{k'}|^2}{2K} \\ &\quad - \frac{k_\parallel'k_\theta' g}{\gamma_\mu'\gamma_\eta'\gamma_\chi' k_\perp'^2}\frac{|k_\perp'^2 A_{k'}\phi_{k'}|}{2K}, \end{aligned} \tag{15}$$

$$\eta_N = \sum_{k'} \frac{1}{\gamma_\eta'}\left(1 - \frac{k_\parallel'^2 k_\perp'^2 + k_\parallel'k_\theta'\frac{dJ_0}{dr}}{k_\perp'^2}\right)\frac{|k_\perp'\phi_{k'}|^2}{2K}, \tag{16}$$

$$\chi_N = \sum_{k'} \frac{1}{\gamma_\chi'}\left(1 - \frac{k_\theta' g\frac{dp_0}{dr}}{k_\perp'^2\gamma_\chi'\gamma_\mu'}\right)\frac{|k_\perp'\phi_{k'}|^2}{2K}, \tag{17}$$

with

$$K = 1 + \frac{k_\parallel'^2 k_\perp'^2 + k_\parallel'k_\theta'^2\frac{dJ_0}{dr}}{k_\perp'^2\gamma_\mu'\gamma_\eta'} + \frac{k_\theta' hg\frac{dp_0}{dr}}{k_\perp'^2\gamma_\mu'\gamma_\chi'}, \tag{18}$$

$$\gamma_\mu' = \gamma' + \mu_c k_\perp'^2 + \mu_N k_\perp'^2, \tag{19}$$

$$\gamma_\eta' = \gamma' + \eta_c k_\perp'^2 + \eta_N k_\perp'^2, \tag{20}$$

$$\gamma_\chi' = \gamma' + \chi_c k_\perp'^2 + \chi_N k_\perp'^2. \tag{21}$$

Here $h = \beta_0/2\epsilon$, β_0 is the plasma beta value, k_θ is the poloidal wave number. In a strong turbulence limit, these coefficients are proportional to the microscopic turbulence level.

The further simplification of eddy viscosities are possible if we specify the background mode and the test mode. In this thesis, we assume that the background mode which represents the microscopic turbulence has the short wavelength and that the mode is quasi-localized.(i.e. with small $k'_{\parallel}$) For the test mode, we consider the conventional tearing mode which is localized around the mode rational surface. Taking the limiting case of wave numbers as, $k'_{\perp} \to \infty$, $k_{\parallel} \to 0$ and $k'_{\parallel} \to 0$, the following relation is obtained for these coefficients

$$\mu_N : \eta_N : \chi_N \sim \frac{1}{3} : 1 : 1, \qquad (22)$$

where the relation $\gamma'_{\mu} \sim \gamma'_{\eta} \sim \gamma'_{\chi}$ is used to derive this relation. In this limit, the electromagnetic terms with $A_{k'}$ vanish and the electrostatic terms with $\phi_{k'}$ survive in the renormalized viscosities.

By this procedure, the effect of microscopic turbulence on the MHD mode is reduced to the renormalized turbulent diffusivities and a two hierarchical model is derived. Using these equations (12)-(14) and (22), we investigate the nonlinear growth rate of tearing mode in the next chapter.

5. Numerical analysis of the tearing mode

In this chapter, the stability of tearing mode immersed in a microscopic turbulence is numerically analyzed by use of model equations (12)-(14). Tearing mode is analyzed in cylindrical coordinates (r, θ, z).

The Fourier representation of perturbation is given by

$$f(\vec{x}, t) = \sum_{m,n} f_{m,n}(r) e^{(i(m\theta + n\frac{z}{R_0}) + \gamma_{m,n} t)}, \qquad (23)$$

where m is the poloidal mode number, n is the toroidal mode number, R_0 is the major radius and $\gamma_{m,n}$ is the growth rate of the tearing mode. In equation (23), the periodic boundary conditions are assumed for the poloidal and toroidal directions and $f_{m,n}(r)$ satisfies the boundary condition; $f_{m,n}(0) = 0$, $f'_{m,n}(0) = 0$ and $f_{m,n}(a) = 0$. Substituting equation (23) into equations (12)-(14), coupled eigenvalue equations are obtained. These equations are numerically solved by the following procedure; as the first step, we solve them by an initial value code to obtain the growth rate, then the parameter dependences are investigated by using the eigenvalue code.

Plasma parameters of middle size tokamak are used, such as the minor radius $a = 0.4$m, the major radius $R_0 = 1.2$m, the toroidal magnetic field $B = 1$T, the electron temperature $T_e = 1.5$kev and the density $n_0 = 2 \times 10^{19} m^{-3}$. For these parameters collisional diffusivities are estimated [17] as $\mu_c = 3.5 \times 10^{-9}$, $\chi_c = 1.3 \times 10^{-9}$, $\eta_c = 2.2 \times 10^{-8}$. In this study, a single helicity mode with m=2/n=1 is analyzed.

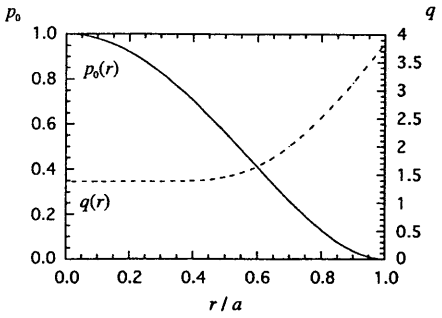

Fig. 11 The equilibrium radial profiles of safety factor $q(r)$ and pressure $p_0(r)$. The rational surface of $m = 2/n = 1$ mode is located near $r_s = 0.7a$.

5.1 Dependence of the growth rate on turbulent diffusivity

The dependence of the growth rate on turbulent diffusivity is studied in this section. The radial profiles of equilibrium safety factor $q(r)$ is chosen as $q(r) = 1.38(1 + (r/0.6a)^8)^{0.25}$, where $q(0) = 1.38$ and $q(a) = 3.8$. In this case, the rational surface of $m = 2/n = 1$ mode is located near $r = 0.7a$. The equilibrium pressure profile is given by $p(r) \propto (1 - (r/a)^2)^2$. They are shown in Figure 11. The equilibrium current profile is calculated from the q profile as,

$$J_0(r) = -\frac{1}{r}\frac{d}{dr}\left(\frac{r^2}{q(r)}\right). \qquad (24)$$

The profile of turbulent diffusivity as well as that of collisional diffusivity are assumed to have a form

$$\eta_N(r) = \hat{\eta}\frac{J_0(r_s)}{J_0(r)}, \qquad (25)$$

where $\hat{\eta}$ is the diffusivity at the rational surface. This profile ensures that the toroidal electric field is uniform, i.e., $E_{\parallel} = \eta J_0$. The same radial profile is assumed for the other diffusive coefficients. It should be noticed that due to the nature of tearing mode the diffusivities have influence on the mode only near the rational surface and the profile effect is less important. Figure 12 shows typical profiles of $m = 2/n = 1$ mode perturbations $\{\phi, A, p\}$ where the turbulent diffusivities are chosen as $\mu_N = \eta_N = \chi_N = 10^{-5}$. The rational surface of $m = 2/n = 1$ mode is located at $r_s = 0.7a$. The derivative of vector potential $A(r)$ is discontinuous at the rational

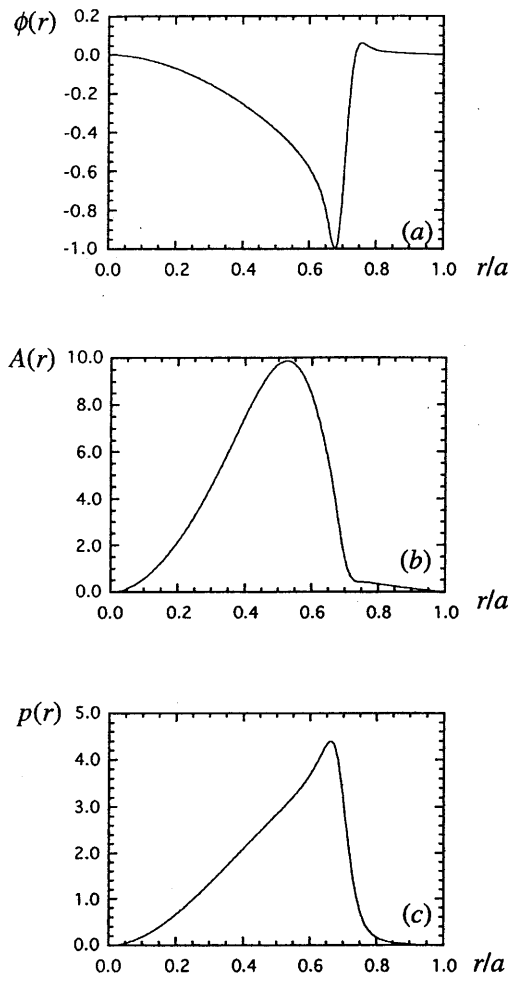

Fig. 12 Typical radial profiles of tearing mode in the cylindrical coordinate. Turbulent diffusivities is chosen as $\mu_N = \eta_N = \chi_N = 10^{-5}$. The rational surface of the mode $m/n = 2/1$ is located near $r_s = 0.7a$. The derivative of vector potential is discreate near r_s.

surface, which is the characteristics of the tearing mode. Δ' indicates the jump of derivative of vector potential A at the rational surface and is defined as

$$\Delta' \equiv \frac{A'(r_s+0) - A'(r_s-0)}{A(r_s)}. \qquad (26)$$

$\Delta' > 0$ indicates that the tearing mode is unstable [18, 19].

In our model, the interchange effect caused by the magnetic curvature is also included, since there exists g in the right hand side of equation (12). The dependence of the mode growth rate on the effective curvature g is investigated and result is shown in Figure 13. The turbulent diffusivities are chosen as $\mu_N = \eta_N = \chi_N = 10^{-5}$. The growth rate is independent of g in the region $g \simeq 0$, which corresponds to the pure tearing mode driven by plasma current. The dependence of the growth rate on g indicates $\gamma \propto g^{0.5}$ in the region $g > 10$, the mode in this parameter range corresponds to ideal interchange mode. The mixing mode occurs for $0 < g < 10$. To analyze the mixing mode which is driven by not only plasma current but also pressure gradient, $g = 2$ is used in this section.

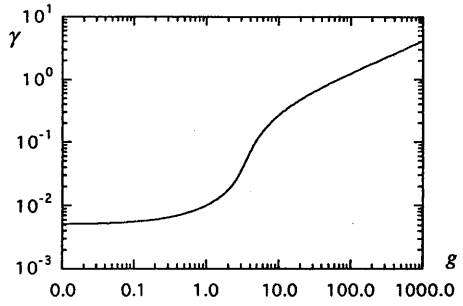

Fig. 13 The dependence of the growth rate on interchange effect g. The turbulent diffusivites is chosen as $\mu_N = \eta_N = \chi_N = 10^{-5}$. As g is greater, the mode becomes pure tearing mode($g \to 0$), mixing mode, and ideal interchange mode(g ¿ 10).

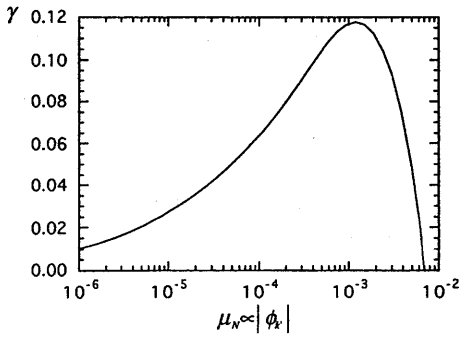

Fig. 14 The dependence of growth rate of tearing mode on turbulent diffusivity, when eqs.(22) is satisfied.

Figure 14 shows the growth rate of tearing mode versus the turbulent diffusivity μ_N which satisfies the relation (22). This result shows that a finite amplitude of microscopic turbulence enhances the growth rate of tearing mode. For the typical parameters, we see that $\mu_N \sim 1m^2/s$ ($\sim 10^{-5}$ as normalized value) corresponds to the growth rate $\gamma_N \sim (30\mu s)^{-1}$. This time scale is almost the same order as ones observed in various types of collapse phenomena [1]. On the other hand, the linear growth rate of tearing mode destabilized by collisional resistivity is about 10^{-2} times smaller and is almost zero since the collisional viscosities are too small, which are of the order of $\mu_c \sim \chi_c \sim \eta_c \sim 10^{-8}$. It should be noted that the nonlinear growth rate is much larger than the linear growth rate of tearing mode. At very high level of turbulent diffusivity, i.e., $\mu_N \sim 10^{-2}$, the nonlinear marginally stability point, $\gamma = 0$, exists. To explore the stability mechanism of this tearing mode, the effect of each duffusivity on the mode is studied in the neighborhood of marginal stability.

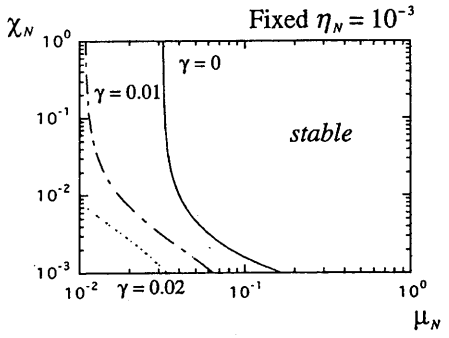

Fig. 15 The contour plot of the growth rate γ in the case that μ_N and χ_N vary independently and $\eta_N = 10^{-3}$ is fixed.

Figure 15 shows the contour plot of the growth rate γ on the (μ_N, χ_N) plane. The case that μ_N and χ_N vary independently and η_N is fixed at 10^{-3} is studied. The solid line indicates the marginal stability condition to μ_N and χ_N for fixed η_N. As the values of μ_N and χ_N increase, the growth rate reduces. This result indicates that μ_N and χ_N stabilize the tearing mode. Physically, it means that the kinetic energy of fluids is released by the turbulent viscosity and thermal conductivity.

The effect of η_N on the growth rate is also studied. Figure 16 shows the contour plot of the growth rate γ_N on the (μ_N, χ_N) plane in the case that η_N and χ_N vary independently keeping the relation $\mu_N = \chi_N$ to hold. It is well known that the tearing mode is

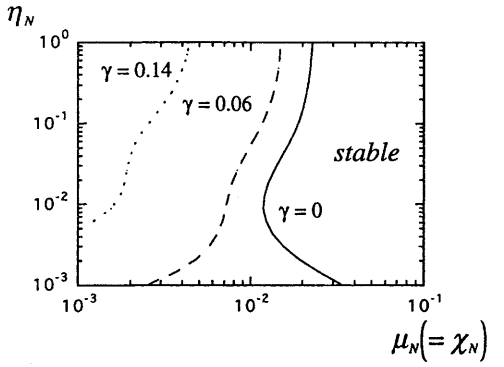

Fig. 16 The contour plot of the growth rate γ in the case that μ_N and η_N vary independently and that the relation $\chi_N = \mu_N$ hold.

destabilized by the collisional resistivity [18]. However, near the marginal stability boundary $\gamma = 0$, there is a parameter region where the growth rate reduces as η_N increase. The region where η_N stabilizes the tearing mode is newly found. It should be noticed that this is different from the one with the relation (22), where only the destabilizing effect of η_N exists. Usually, turbulent diffuivities are of order $1m^2/sec$ in tokamak plasma, therefore it may be not realistic to approach this marginal stability point. However, in reversed field pinch plasma where a strongly enhanced transport of order $\chi_N \sim 10^3 m^2/sec$ is observed, it could be realistic.

5.2 Resistive ballooning mode as a micro-turbulence

Resistive ballooning mode (RBM) turbulence is chosen as a background micro-turbulence in this section. The stability of the tearing mode is examined and the parameter dependences are investigated. We assume that the background turbulence is driven by collisionality, which ensures the closure of hierarchy. The microscopic turbulence is driven by the collisional resistivity and acts on the global MHD mode through the turbulent eddy diffusivity which is larger than the classical resistivity by factor of 10 $\sim$ 100 for typical parameters.

The turbulent diffusivity of RBM [20] is given as,

$$\chi_N = C_0 \frac{\alpha}{s} \eta_c, \tag{27}$$

where $\alpha = -q^2\beta'/\epsilon$ is the ballooning parameter, $s = rq'/q$ is the shear parameter and C_0 is a numerical constant. η_N and μ_N are given from the relation (22). Parameters such as s and α affect the growth rate of tearing mode through the turbulent diffusivities, μ_N, η_N and χ_N. The growth rate of the tearing mode enhanced

by RBM turbulence is calculated by

$$\gamma_N^{RBM} \propto (\Delta')^{\frac{4}{5}}(\eta_N)^{\frac{3}{5}}s^{\frac{2}{5}} \propto (\Delta')^{\frac{4}{5}}\frac{\alpha^{\frac{3}{5}}}{s^{\frac{1}{5}}}\eta_c^{\frac{3}{5}}, \quad (28)$$

which shows that s has a stabilizing effect and α has a destabilizing effect on the growth rate. On the contrary, the growth rate of classical tearing mode is given as

$$\gamma_{classical} \propto (\Delta')^{\frac{4}{5}}(\eta_c)^{\frac{3}{5}}s^{\frac{2}{5}}. \quad (29)$$

which means that the classical tearing mode is destabilized by the magnetic shear s.

In order to examine the discrepancy between the RBM turbulent driven tearing mode and the classical tearing mode, the magnetic shear dependence is investigated. To this end, the safety factor profile, i.e., the equilibrium current profile is changed. Other parameters are fixed as $C_0 = 10$, $\eta_c = 2.2 \times 10^{-7}$, $\mu_c = 3.5 \times 10^{-8}$, $\chi_c = 1.5 \times 10^{-8}$. Shear dependence is investigated for the limiting case $g = 0$ to compare with the analytical result of pure tearing mode. Figure

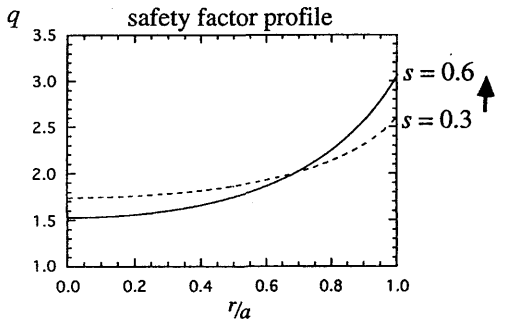

Fig. 17 Typical $q(r)$ profiles when $s = 0.3, 0.6$. The location of rational surface of $m = 2/n = 1$ mode is fixed near $r_s = 0.7a$.

17 shows the typical safety factor profiles in cases with $s = 0.3, 0.6$ at $r/a = 0.7$. The dependence of shear on the growth rate is calculated in the range $0.1 < s < 0.6$. This result is shown in Figure 18. Solid line indicates the growth rate of the tearing mode driven by RBM turbulence. Dotted line shows the case of classical tearing mode. In the presence of RBM turbulence, as s becomes large γ reduces for $s > 0.13$. The magnetic shear stabilizes the tearing mode through the turbulent diffusivities. This is expected by the analytical estimation (28). In the low-shear limit, a region appears where the magnetic shear destabilizes the tearing mode through the RBM turbulence. This may be understood in the following. The RBM turbulent diffusivities are so large in the low-shear limit that the effect of turbulent viscosity

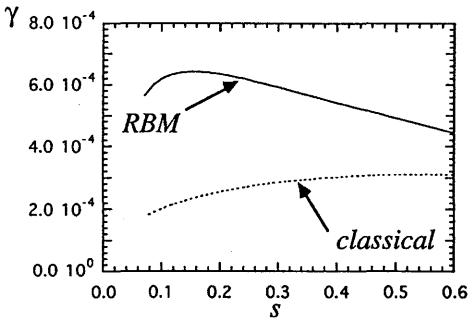

Fig. 18 The dependence of the growth rate on shear parameter with/without the resistive ballooning mode turbulence. Solid line indicates the case with RBM turbulence. Dotted line shows the case of classical tearing mode which is driven by collisional resistivity.

and turbulent thermal conductivity, which stabilizes the tearing mode, can not be neglected. They are not taken into account in the analytical estimation (28).

α dependence is also studied for the finite value of g case. $g = 0.01$ is chosen to clarify the difference between the classical case and the RBM turbulence case. Figure 19 shows the contour plot of the growth rate γ on the (s, α) plane. To analyze the dependence of the growth rate on α, beta value at the center i.e. $\beta(0)$ is changed. The result of tearing mode with resistive ballooning mode turbulence is shown in Figure 19(a). Figure 19(b) shows the case of classical tearing mode which is driven by the collisional resistivity. In the region $s \simeq \alpha (s > 0.2)$, the difference is clear, i.e., there is no contour line in this region for the case of classical tearing mode 19(b). On the other hand, there are the contour lines for of constant γ for the case with RBM turbulence 19(a). This result shows that the tearing mode in the case with RBM turbulence is destabilized by α and stabilized by s.

6. Summary and Discussion

In this thesis, the nonlinear interaction between a global MHD mode and a background microscopic turbulence is considered. A new driving mechanism of global MHD mode is presented and analyzed. As an example, the stability analyses of tearing mode immersed in the microscopic turbulence are performed. The effects of microscopic turbulence are introduced as the turbulent drags to the tearing mode. These nonlinear effects are approximated by the one-point renormalization method. Nonlinear terms are further reduced to transport coef-

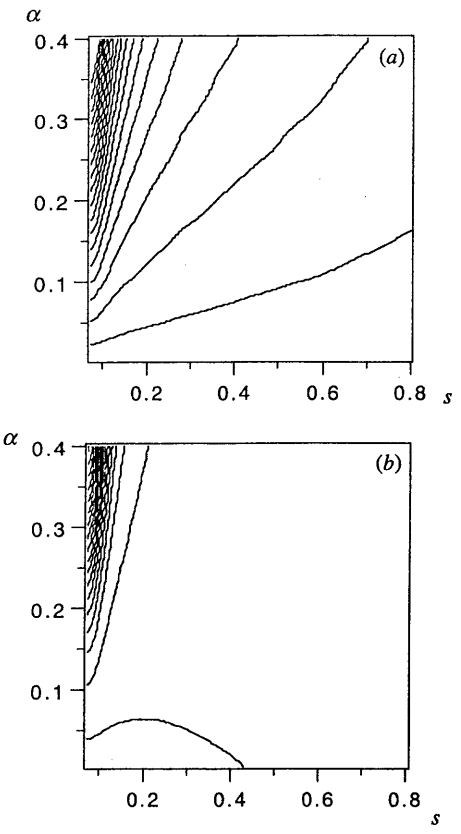

Fig. 19 The contour plot of the growth rate on $s-\alpha$ plane with the resistive ballooning turbulence case (a) and classical case (b), where tearing mode is driven by collisional resistivity. The effective curvature is chosen as $g = 0.01$. In the case of RBM turbulence, α destabilizes and s stabilizes tearing mode in wide region comparing with classical case.

ficients by use of the mean-field approximation and the diffusion approximation. Model equations for the global MHD mode in the presence of microscopic turbulence are thus derived. If one considers the limit, $k'_\perp \to \infty$, $k'_\parallel \to 0$ and $k_\parallel \to 0$, the relation equation (22) of these coefficients is derived.

Using these model equations, the dependence of the growth rate of tearing mode on turbulent diffusivity is analyzed. It is shown that a finite amplitude of microscopic turbulence enhances the growth rate of tearing mode. For the typical parameters of middle size tokamak, it is found that $\mu_N \sim 1m^2/s$ corresponds to the growth rate $\gamma_N \sim (30\mu s)^{-1}$. This time-scale is the similar order to the fast time-scale of sudden growth observed in various types of collapse phenomena in the high temperature plasmas. This result may give an insight for the mechanism of sudden growth of tearing mode in a collisionless regime.

The effect of turbulent diffusivity on tearing mode is studied near the marginal stability boundary. It is shown that ion viscosity μ_N and thermal diffusivity χ_N stabilize the tearing mode, while the resistivity η_N generally destabilizes it. However, a region where η_N tends to stabilize the tearing mode is newly found in the neighborhood of the marginal stability boundary.

Turbulent diffuivities which are observed as the anomalous transport are usually of order $1m^2/sec$ in tokamak plasma, therefore it is not realistic to access the marginal stability point. However, in reversed field pinch plasma where a strongly enhanced transport of order $\chi_N \sim 10^3 m^2/sec$ is predicted, it could be realistic.

The tearing mode in the presence of resistive ballooning turbulence is studied. The results show that the shear parameter s stabilizes the pure tearing mode($g = 0$) in high shear region, where the classical tearing mode is known to be destabilized by the magnetic shear. The finite g case is also studied to analyze the effect of pressure gradient. The results show that tearing mode is destabilized by α and stabilized by s through RBM turbulence in the region where classical tearing mode is little affected by s and α. These results indicate that instabilities driven by microscopic turbulence could have different dependence on global parameters from the one without the turbulent drag.

This study analyzes the initial phase of the growth of tearing mode. Also, the microscopic turbulence can have an influence on the magnetic island growth. The growth of magnetic island is analyzed in Ref [12], where the growth of perturbed flux function $\tilde{\psi}$ is given as

$$\frac{\partial \tilde{\psi}}{\partial t} \propto \Delta \eta \tilde{\psi}^{\frac{1}{2}}. \qquad (30)$$

Therefore, the anomalous resistivity could affect the growth of magnetic island. The effects of ion viscosity and thermal conductivity are not taken into account in this equation 30. In our model, turbulent diffusivities μ_N, η_N and χ_N are the same order quantities and also μ_N and χ_N have an influence on the island width. Analysis of the magnetic island with background turbulence in the Rutherford regime is needed and left for a future work.

7. Acknowledgement

This work is partly supported by the Grant-Aid for Scientific Research of the Ministry of Education, Science, Sport and Culture in Japan and by collaboration programme of Advanced Fusion Research Center/RIAM of Kyushu Unversity.

References

1) Itoh, S.-I., Itoh, K., Zushi, H. and Fukuyama, A.: *Plasma Phys. Control. Fusion*, Vol.40, (1998) 879

2) Goeler, S.V., Stodiek, W. and Sauthoff, N.:*Phys. Rev. Lett.*, Vol.33, (1974)1201

3) Compbell, D.J., et al.:*Plasma Phys. Control. Nucl. Fusion Res.*, Vol.1(Vienna: Vienna), (1986)433

4) Artsimovich, L.A.: *Nucl. Fusion*, Vol.12, (1972)215

5) JET Team(presented by Campbell, D.J.): *Plasma Phys. Control. Fusion Res.*, Vol.3(Seville: IAEA), (1991)231

6) Zushi, H., et al.: Fusion energy *Proc. 16th Int. Conf. on Fusion Energy(1996)* Vol.2(Vienna: IAEA), 143

7) McGuire, K.M. and Robinson, D.C.: *Nucl. Fusion*, Vol.19, (1979)505

8) Diamond, P.H., Hazeltine, An, Z.G., et al.:*Phys. Fluids*, Vol.27, (1984)1449

9) Dupree, T.H.: *Phys. Fluids*, Vol.9, (1966)1773

10) Yagi, M., Itoh, S.-I., Fukuyama, A. and Itoh, K.: *7th IAEA Technical Committee Meeting on H-mode Physics and Transport Barriers, Oxford, Sept. 1999* to be published in a special issue of plasma physics & controlled fusion.

11) Lichtenberg, A.J., Itoh, K., Ioth, S.-I. and Fukuyama, A.: *Nucl. Fusion*, Vol.32, (1992)495

12) Rutherford, P.H.:*Phys. Fluids*, Vol.16, (1973)1903

13) Biglari, H., Diamond, P.H. and Terry, P.W.:*Phys. Fluids* , (1990)1

14) Strauss, H.: *Phys. Fluids*, Vol.20, (1977)1354

15) Itoh, K., Itoh, S.-I. and Fukuyama, A.:*Transport and Structural Formation in Plasmas*, published by IOP Publishing (1999)

16) Itoh, K., Itoh, S.-I., Fukuyama, A., Yagi, M. and Azumi, M.:*Plasma Phys. Control. Fusion*, Vol.36, (1994)279

17) Braginskii, S.I., in Review of Plasma Physics, consultants Bureau, New York, Vol.1, (1985)

18) Furth, H.P., Killeen, and Rosenbluth : *Phys. Fluids*, Vol.6, (1963)459

19) Furth, H.P., Rutherford, P.H. and Selberg, H.:*Phys. Fluids*, Vol.16, (1973)1054

20) Conner, J.W.:*Plasma Phys. Control. Fusion*, Vol.30, (1988)619